Published in final edited form as:

Nat Nanotechnol. 2010 September ; 5(9): 655–659. doi:10.1038/nnano.2010.154.

Very large magnetoresistance in graphene nanoribbons

Jingwei Bai[1,*], **Rui Cheng**[1,*], **Faxian Xiu**[2], **Lei Liao**[3], **Minsheng Wang**[2], **Alexandros Shailos**[4], **Kang L. Wang**[2,4], **Yu Huang**[1,4], and **Xiangfeng Duan**[3,4]

[1]Department of Materials Science and Engineering, University of California, Los Angeles, California 90095, USA.

[2]Department of Electrical Engineering, University of California, Los Angeles, California 90095, USA.

[3]Department of Chemistry and Biochemistry, University of California, Los Angeles, California 90095, USA.

[4] California Nanosystems Institute, University of California, Los Angeles, California 90095, USA.

Abstract

Graphene has unique electronic properties1,2 and graphene nanoribbons are of particular interest because they exhibit a conduction band gap, which arises due to size confinement and edge effects3-11. Theoretical studies have suggested that graphene nanoribbons could have interesting magneto-electronic properties with very large magnetoresistance predicted4,12-20. Here we report the experimental observation of a significant enhancement in the conductance of a graphene nanoribbon field-effect transistor in a perpendicular magnetic field. A negative magnetoresistance of nearly 100% was observed at low temperatures, with over 50% remaining at room temperature. This magnetoresistance can be tuned by varying the gate or source-drain bias. We also find that the charge transport in the nanoribbons is not significantly modified by an in-plane magnetic field. The large values of the magnetoresistance we observe may be attributed to the reduction of quantum confinement by the formation of cyclotron orbits and the delocalization effect under the perpendicular magnetic field15-20.

Our graphene nanoribbon field-effect transistors (FETs) are fabricated using SiO_2 nanowires as physical etching masks (see Methods for details)11. A typical device uses a narrow graphene nanoribbon as a semiconducting channel with the width determined by the mask nanowire diameter and the length defined by *e*-beam lithography. The source and drain contacts are formed by *e*-beam evaporation of Ti/Au film covering graphene blocks. A highly *p*-type doped Si wafer are used as the back gate with a 300 nm thick SiO_2 as the gate

---

Correspondence and requests for materials should be addressed to X.D. (xduan@chem.ucla.edu) and Y.H (yhuang@seas.ucla.edu)..

*These authors contribute equally to this work.

Author Contributions X.D, Y.H., J.B., R.C. and L. L. conceived and designed the experiments. J.B., C.R. and F. X. performed the experiments. J.B. and C.R. collected and analyzed the data. M.W., A.S. and K.W. contributed experimental tools, J.B., C.R. Y.H. and X.D. co-wrote the paper. All authors discussed the results and commented on the manuscript.

Additional information Supplementary Information accompanies the paper on www.nature.com/naturenanotechnology. Reprints and permission information is available online at http://npg.nature.com/reprintsandpermissions.

dielectric (Figure 1). Unlike conventional *e*-beam lithography defined graphene nanoribbons in which polymeric resist residue may heavily dope the nanoribbons and results in large positive shift of charge neutrality point21, the graphene nanoribbons obtained with our method show relatively neat performance with charge neutrality points typically in the range of 0-5 V in the back-gate configuration21.

The electrical transport characteristics of the graphene nanoribbon devices were typically carried out at 1.6 K unless mentioned otherwise. The black line in Figure 2a shows a differential conductance with respect to the gate voltage for a typical nanoribbon device with channel width of ~15 nm and length of 800 nm. The curve indicates a strong suppression of conduction in this relatively long device with a transport gap in the gate region of 0.4 to 6.6 V. Figure 2b further shows differential conductance as a function of both the gate voltage and the source-drain bias; a diamond like characteristics of suppressed conductance consisting of a number of sub-diamonds is clearly seen. In particular, smaller diamonds are also observed away from the main transport gap region (Figure 2b), indicating that the charge transport in our device is related to the model of multiple graphene quantum dots in series along the nanoribbon22-26. The formation of the quantum dot structure in the nanoribbons may be attributed to edge roughness or local potential variation5,8,22,23.

We also performed the magneto-transport measurements under a magnetic field up to 8 T normal to the device plane. Previous magnetoresistance study of large graphene flakes showed a non-saturated positive magnetoresistance near the minimum conductance point, representing carrier transport through inhomogeneously distributed electron and hole puddles of equal mobility27,28. In contrast, our graphene nanoribbon device exhibits very large negative magnetoresistance that is highly dependent on the exact gate voltage and source-drain bias. Upon applying a magnetic field, the overall conductance increases dramatically with a much reduced transport gap in the gate sweep (red curve in Figure 2a). Near the edge of the original transport gap (back gate voltage (V_g) range 0.4~1.9 V and 4.6~6.6 V), the differential conductance is essentially switched on from a completely off state upon applying a magnetic field (8 T) with a differential conductance increase up to 1000 fold or more. On the other hand, the average conductance rises about 2-4 times when the device is gated far away from the transport gap region ($V_g < 0.4$ V or $V_g > +6.6$ V). This phenomenon is more evident in the two dimensional differential conductance plots as shown in Figure 2b-d: the overall diamond of suppressed conductance shrinks significantly in both the gate and source-drain bias directions, and those sub-diamonds at the edge of the transport gap region become so conductive that the transport gap reduces to 1.9-4.6 V in gate sweep at 8 T.

Figure 3a further shows the current-voltage (*I*-*V*) characteristics near the charge neutrality point at different magnetic fields. The *I*-*V* curves exhibit non-linear behaviour near zero source-drain bias, in which the semiconducting like nonlinear gaps denoted as source-drain gap decrease from 25 meV at 0 T to 4.3 meV at 8 T (Figure 3a inset). Note that the source-drain gap is defined by a steep increase of current in logarithmic scale (Figure S1)23. These results suggest that the transport barrier decreases with the increase of the magnetic field9,23. At the edge of the transport gap (Figure 2b, V_g=1 V) where the sub-diamonds of the suppressed conductance nearly disappear at high magnetic field, the source-drain

conduction gap decreases from 16.6 to 0.5 meV (Figure 3b inset). Further away from the charge neutrality point (V_g=0 V), the magnetic field has less effect on the device current, although significant change can still be observed, for example, near zero source-drain bias in the small source-drain gap region, which almost totally disappeared at 8 T (Figure 3c and inset).

The *I-V* characteristics indicate that the huge magnetoresistance can be readily obtained by tuning the exact electronic states of the device. Figure 3d plots the current ratio of I(8T)/I(0T) versus source-drain bias at V_g = 0, 1 and 3 V. All three curves show large increase of current ratio when approaching the transport blockade region. Significantly, over 4 orders of magnitude of increase in current can be observed at the edge of the blockade. This exceptionally large magnetoresistance cannot be well described using conventional formula: magnetoresistance = $\Delta R/R_0$ because current ratio of over 100 already gives magnetoresistance of -99%, while 4 orders of magnitude change gives an magnetoresistance value of -99.99%. To better examine the magnitude of the conductance change, we simply use current (conductance) ratio to describe the exceptionally large magnetoresistance in our device. Figure 3d clearly shows that the current ratio can be tuned from a few times up to >10,000 times, depending on the exact gate or source-drain bias. Similar scenarios were also observed in the electron-transport branch (Figure S2). Additionally, we have fabricated and studied more than ten devices, and all of them exhibit similar negative magnetoresistance (Figures S3-S5).

Figure 3e provides a general view of current ratio as a function of both the source-drain bias and gate voltage, which further demonstrates the tunability of the magnetoresistance observed in our graphene nanoribbon devices. In general, the current ratio increases significantly when the device is tuned to the proximity of the diamond blockade region and reaches the highest value at the edge of the conductance suppressing diamond. Within the diamond, the magnetoresistance value cannot be accurately determined because the current through the device is below our equipment measurement capability. Figure 3f shows the magneto-response at gate voltage of 1 V at different source-drain bias. In general, the current ratios increase more rapidly with magnetic field when biased closer to the blockade region. In all cases, the current increases exponentially and shows no evidence of saturation up to 8 T (Note that the figure is in exponential scale).

Electric field control of magnetoresistance has recently attracted considerable attention in multifunctional logic devices. Several material systems, including carbon nanotubes, semiconductor quantum dots and nanowires coupled with ferromagnetic (FM) electrodes, have been explored in this regard but only with limited tunability achieved to date29-31. Importantly, our studies demonstrate that graphene nanoribbons themselves without artificially engineered ferromagnetic contacts can exhibit extraordinary magnetoresistance (nearly -100% with current ratio over 10,000) that is highly tunable by either varying the gate voltage or source-drain bias, thus enabling an entirely new material system and device structure for multifunctional magnetic logic device.

We have also studied the magnetoresistance evolution with increasing temperature. Figure 4a and 4b show the current ratio and negative magnetoresistance versus source-drain bias at

variable temperatures at V_g = 3 V. The maximum current ratio decreases from more than 10,000 at 1.6 K, to nearly 20 (magnetoresistance = -95%) at 25 K, and to 3 (magnetoresistance = -70%) at 77 K, as the conductance suppression due to conduction band gap and/or Coulomb blockade effect is weakening with the increase of temperature. The conduction band gap apparently disappears at room temperature as the device shows linear transport behaviour (Figure 4c). At this point, the magnetoresistance can no longer be modified by source-drain bias voltage, and is also only weakly tunable by gate voltage. Nonetheless, the negative sign of magnetoresistance persists up to room temperature. A nearly linear increase of magnetoresistance with magnetic field and up to -56 % magnetoresistance is obtained at 8 T at V_g = 3 V (inset of Figure 4c). For practical considerations, it is valuable to note the magnetoresistance at low magnetic field. The room temperature magnetoresistance reaches ~ 4% at a low magnetic field of 0.5 T, which is not as striking as low temperature data (up to 50 % at 0.5 T), but is still very significant in a device with no ferromagnetic materials. It is now well known that the conduction band gap of graphene nanoribbon is inversely proportional to the ribbon width, and sub-5 nm nanoribbons can develop large enough conduction band gap to completely shut off the conductance even at room temperature9-11. Based on our observation of magnetoresistance enhancement near the conductance suppression diamond, larger magnetoresistance at room temperature may be achievable when ribbon width is further shrunk down to the sub-5 nm regime.

To further elucidate the magnetoresistance effect in our device, we have fabricated shorter channel graphene nanoribbon device with channel length of 200 nm, aiming to reduce the number of quantum dots along the nanoribbon device22. Indeed, simpler transport characteristics with better resolved Coulomb blockade structures were observed in this shorter device (Figure 5a), although the jointed diamonds still indicated multiple coulomb blockade effect20. Upon applying a magnetic field of 3 T and 6 T, the shrinkage of each diamond is clearly seen (Figure 5b, c). The size of the diamond structure (bias gap) shrinks consistently with increasing magnetic field (Figure S6). The gate sweeps show overall conductance increase: the conductance peak grows and broadens; and conductance valley arises, resulting in a diminishing of the blockade region (Figure 5d). Interestingly, the blockade position is not significantly shifted with magnetic field up to 3 T, indicating no significant change of quantum dot configuration. These diamonds almost disappear when the magnetic field is increased to 6 T, suggesting that charge hopping through the nanoribbon can be significantly enhanced under an external magnetic field.

Previous theoretical studies have predicted interesting magneto-transport properties in graphene nanoribbons with multiple possible origins. For example, first-principle calculations have predicted the existence of semiconducting antiferromagnetic spin state in the zigzag graphene nanoribbons that can be excited to metallic ferromagnetic state with an applied magnetic field12-14. However, this possibility was eliminated in our devices by performing magnetoresistance measurement with an in-plane magnetic field in which no obvious magnetic response was found (Figure S7). On the other hand, recent theoretical studies indicate that a perpendicular magnetic field can greatly modify lateral quantum confinements in graphene nanoribbons and profoundly impact the charge transport due to the formation of cyclotron orbits originated from Dirac-Landau-level behaviour in the

graphene nanoribbons15-20. It is suggested that a perpendicular magnetic field can induce cyclotron orbits of the electrons motion with the cyclotron length $l_B = (\hbar/eB)^{-1/2}$, where e is the electron charges and B is magnetic field. At lower magnetic field with large cyclotron length, the cyclotron wavefunction extends beyond the ribbon width, electron motion is strongly affected by the ribbon edges and the quantum confinement dictates the electrical properties of the graphene nanoribbons. With increasing magnetic field, the cyclotron length decreases. When the cyclotron length becomes comparable or smaller than ribbon width, the ribbon edges and confinement potential become less relevant in the ribbon electrical properties, and it would eventually completely eliminate the edge confinement to induce a semiconductor-metal transition at high enough magnetic field17-19. Recent tight-binding calculations have shown the confinement band gap of semiconducting armchair graphene nanoribbons indeed shrinks continuously with increasing magnetic field17. The cyclotron length $l_B = (\hbar/eB)^{-1/2}$ is 26.6 nm at 1 T and 9.4 nm at 8 T, comparable to our nanoribbon widths, suggesting that the magnetic field can indeed significantly modify the electronic structure and charge transport in our graphene nanoribbon devices.

In a typical graphene nanoribbon with multi-coulomb blockade transport characteristics due to experimental edge roughness and local potential variation, the confinement gaps function as energy barriers for charge transport across different electron hole puddles along the nanoribbon8,22. Therefore, a decrease of confinement gap with magnetic field can reduce the charge hopping barrier in the multi-coulomb blockade device, and effectively reduce the overall conduction band gap with increasing magnetic field, as we have observed in our devices (inset, Figure 3a). This is also consistent with the evolution of diamond structure in our short channel device, in which the sizes of the Coulomb diamonds clearly shrink with increasing magnetic field. Our temperature dependent studies also show that the thermal activation energy of charge transport in the graphene nanoribbons also decreases with increasing magnetic field, further suggesting the shrinkage of the confinement gaps31 by the perpendicular magnetic field (See supporting materials, Figure S8). Additionally, the edge roughness induced back scattering in terms of strong localization may also contribute to the observed conductance suppression6, in which magnetic field can induce the delocalization effect, suppress the back scattering, and hence enhance the conductance32. The Coulomb blockade effect can significantly enhance the magnetoresistance at the edge of the transport gap/source-drain gap where the charge transport is more sensitive to the magnetic field. On the other hand, when gated or biased outside the transport gap or under high temperature in which current flow is dominated by drifting and the conductance is limited by edge or charge impurity scattering, the observed magnetoresistance is expectedly not as striking as that under tunnelling condition.

In conclusion, we have reported an extraordinarily large tunable magnetoresistance in graphene nanoribbon-FET devices. Negative magnetoresistance nearly 100% with over 10,000 times conductance increase was demonstrated at 1.6 K and negative magnetoresistance nearly 56 % was obtained at room temperature. This magnetoresistance can be readily tuned by gate voltage and source-drain bias in which the enhancement reaches the maxima near the edge of the conduction band gap. Although further experimental and theoretical studies will be necessary to fully elucidate the exact

mechanism responsible for the observed negative magnetoresistance, our experimental findings clearly demonstrate that the graphene nanoribbons exhibit interesting magneto-transport properties and may open exciting opportunities in magnetic sensing and a new generation of magneto-electronic devices. During the manuscript revision and editorial period, we became aware of preprints on similar topics posted on condensed matter arXiv33,34. Our work was developed independently from the work reported in these preprints.

METHODS

The graphene nanoribbon-FETs were fabricated using SiO_2 nanowires as the physical etching masks11. Silicon nanowires with diameters ranging from 5 to 40nm were grown using catalytic chemical vapour deposition, and oxidized in air at 900°C for 15 minutes to produce an SiO_2 insulating shell or fully oxidized nanowires. Graphene flakes were mechanical peeled from natural graphite onto heavily doped p-type silicon wafers with 300 nm thermal oxide. After that, we physically transferred the SiO_2 nanowires from the growth substrate to the graphene substrate via a contact printing approach. Specifically, a graphene device substrate was first firmly attached to a benchtop, and the nanowire substrate was placed upside down on top of the graphene device substrate such that the nanowires were in contact with the graphene. A gentle manual pressure was then applied from the top followed by slightly sliding the growth substrate. The nanowires were transferred onto the graphene device substrate by the sheer forces during the sliding process. The sample was then rinsed with isopropanol followed by nitrogen blow-dry, in which capillary drying process near the nanowires can help them to firmly attach to the graphene flakes. The nanowire position was determined by dark field microscopy or atomic force microscopy. E-beam lithography was used to define source and drain electrodes according to the position of the nanowires on the graphene, and Ti/Au 7nm/90nm film was evaporated with an *e*-beam evaporator. The graphene regions not protected by the nanowires were etched away by oxygen plasma under 30-40W for 20s. Transport measurements were carried out in a pumped liquid He system equipped with a superconducting magnet (American Magnetics, Inc.). Differential conductance (dI/dV) measurements were performed using standard lock-in detection technique in which a superimposed low frequency (17 Hz) ac current modulation was measured as a function of dc voltage bias component.

Supplementary Material

Refer to Web version on PubMed Central for supplementary material.

Acknowledgements

We acknowledge Center for Quantum Research and Nanoelectronics Research Facility at UCLA for technical support. We thank D. Newhauser and Y. Tserkovnyak for discussions. Y.H. acknowledges support from the Henry Samueli School of Engineering and an Applied Science Fellowship. X.D. acknowledges support by NSF CAREER award 0956171 and the NIH Director's New Innovator Award Program, part of the NIH Roadmap for Medical Research, through grant number 1DP2OD004342-01.

Reference

1. Geim AK, Novoselov KS. The rise of graphene. Nature Mater. 2007; 6:183–191. [PubMed: 17330084]
2. Castro Neto AH, Guinea F, Peres NMR, Novoselov KS, Geim AK. The electronic properties of graphene. Rev. Mod. Phys. 2009; 81:109–162.
3. Nakada K, Fujita M, Dresselhaus G, Dresselhaus MS. Edge state in graphene ribbons: Nanometer size effect and edge shape dependence. Phys. Rev. B. 1996; 54:17954–17961.
4. Son YW, Cohen ML, Louie SG. Energy gaps in graphene nanoribbons. Phys. Rev. Lett. 2006; 97:216803. [PubMed: 17155765]
5. Sols F, Guinea F, Neto AHC. Coulomb blockade in graphene nanoribbons. Phys. Rev. Lett. 2007; 99:166803. [PubMed: 17995278]
6. Gunlycke D, Areshkin DA, White CT. Semiconducting graphene nanostrips with edge disorder. Appl. Phys. Lett. 2007; 90:142104.
7. Adam S, Cho S, Fuhrer MS, Das Sarma S. Density inhomogeneity driven percolation metal-insulator transition and dimensional crossover in graphene nanoribbons. Phys. Rev. Lett. 2008; 101:046404. [PubMed: 18764347]
8. Stampfer C, et al. Energy Gaps in Etched Graphene Nanoribbons. Phys. Rev. Lett. 2009; 102:056403. [PubMed: 19257529]
9. Han MY, Ozyilmaz B, Zhang YB, Kim P. Energy band-gap engineering of graphene nanoribbons. Phys. Rev. Lett. 2007; 98:206805. [PubMed: 17677729]
10. Li XL, Wang XR, Zhang L, Lee SW, Dai HJ. Chemically derived, ultrasmooth graphene nanoribbon semiconductors. Science. 2008; 319:1229–1232. [PubMed: 18218865]
11. Bai JW, Duan XF, Huang Y. Rational fabrication of graphene nanoribbons using a nanowire etch mask. Nano. Lett. 2009; 9:2083–2087. [PubMed: 19344151]
12. Son YW, Cohen ML, Louie SG. Half-metallic graphene nanoribbons. Nature. 2006; 444:347–349. [PubMed: 17108960]
13. Kim WY, Kim KS. Prediction of very large values of magnetoresistance in a graphene nanoribbon device. Nature Nanotech. 2008; 3:408–412.
14. Munoz-Rojas F, Fernandez-Rossier J, Palacios JJ. Giant magnetoresistance in ultrasmall graphene based devices. Phys. Rev. Lett. 2009; 102:136810. [PubMed: 19392393]
15. Peres NMR, Castro Neto AH, Guinea F. Dirac fermion confinement in graphene. Phys. Rev. B. 2006; 73:241403.
16. Peres NMR, Castro Neto AH, Guinea F. Conductance quantization in mesoscopic graphene. Phys. Rev. B. 2006; 73:195411.
17. Huang Y, Chang CP, Lin MF. Magnetic and quantum confinement effects on electronic and optical properties of graphene ribbons. Nanotechnology. 2007; 18:495401. [PubMed: 20442470]
18. Liu J, Wright AR, Zhang C, Ma Z. Strong terachertz conductance of graphene nanoribbons under a magnetic field. Appl. Phys. Lett. 2008; 93:041106.
19. Ritter C, Makler SS, Latge A. Energy-gap modulations of graphene ribbons under external fields: a theoretical study. Phys. Rev. B. 2008; 77:195443.
20. Li TS, Huang YC, Chang SC, Chang CP, Lin MF. Magnetoconductance of graphene nanoribbons. Phil. Mag. 2009; 89:697–709.
21. Lin YM, Perebeinos V, Chen ZH, Avouris P. Electrical observation of subband formation in graphene nanoribbons. Phys. Rev. B. 2008; 78:161409.
22. Gallagher P, Todd K, Foldhaber-Gordon D. Disorder-induced gap behavior in graphene nanoribbons. Phys. Rev. B. 2010; 81:115409.
23. Han MY, Brant JC, Kim P. Electron transport in disordered graphene nanoribbons. Phys. Rev. Lett. 2010; 104:056801. [PubMed: 20366782]
24. Ozyilmaz B, Jarillo-Herrero P, Efetov D, Kim P. Electronic transport in locally gated graphene nanoconstrictions. Appl. Phys. Lett. 2007; 91:192107.
25. Scott Bunch JS, Yaish Y, Brink M, Bolotin K, McEuen PL. Coulomb osillations and hall effect in quasi-2D graphite quantum dots. Nano Lett. 2005; 5:287–290. [PubMed: 15794612]

26. Ponomarenko LA, Schedin F, Katsnelson MI, Yang R, Hill EW, Novoselov KS, Geim AK. Chaotic dirac billiard in graphene quantum dots. Science. 2008; 320:356–358. [PubMed: 18420930]
27. Cho S, Fuhrer MS. Charge transport and inhomogeneity near the minimum conductivity point in graphene. Phys. Rev. B. 2008; 77:081402.
28. Martin J, et al. Observation of electron-hole puddles in graphene using a scanning single-electron transistor. Nature Phys. 2008; 4:144–148.
29. Sahoo S, et al. Electric field control of spin transport. Nature Phys. 2005; 1:99–102.
30. Hamaya K, et al. Electric-field control of tunneling magnetoresistance effect in a Ni/InAs/Ni quantum-dot spin valve. Appl. Phys. Lett. 2007; 91:022107.
31. Martin I, Blanter YM. Transport in disordered graphene nanoribbons. Phys. Rev. B. 2009; 79:235132.
32. Gershenson ME, Khavin YB, Mikhalchuk AG, Bozler HM, Bogdanov AL. Crossover from weak to strong localization in quasi-one-dimensional conductors. Phys. Rev. Lett. 1997; 79:725–728.
33. Poumirol JM, Cresti A, Roche S, Escoffier W, Goiran M, Wang XR, Li XL, Dai HJ, Raquet B. Edge magneto-fingerprints in disordered graphene nanoribbons. arXiv. :1002.4571v1.
34. Oostinga JB, Sacepe B, Cracium MF, Morpurgo AF. Magneto-transport through graphene nanoribbons. arXiv. :1003.2994v1.

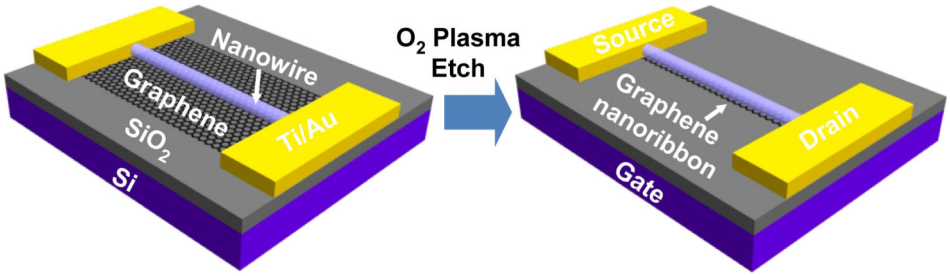

Figure 1. Schematic illustration of fabricating a graphene nanoribbon field-effect transistor using a nanowire as physical etching mask

The device is fabricated on heavily doped silicon substrate with a 300 nm thick SiO_2 as the gate dielectric. *E*-beam lithography defined and *e*-beam evaporation deposited Ti/Au (7 nm/90 nm) film on graphene block is used as the source and drain electrodes.

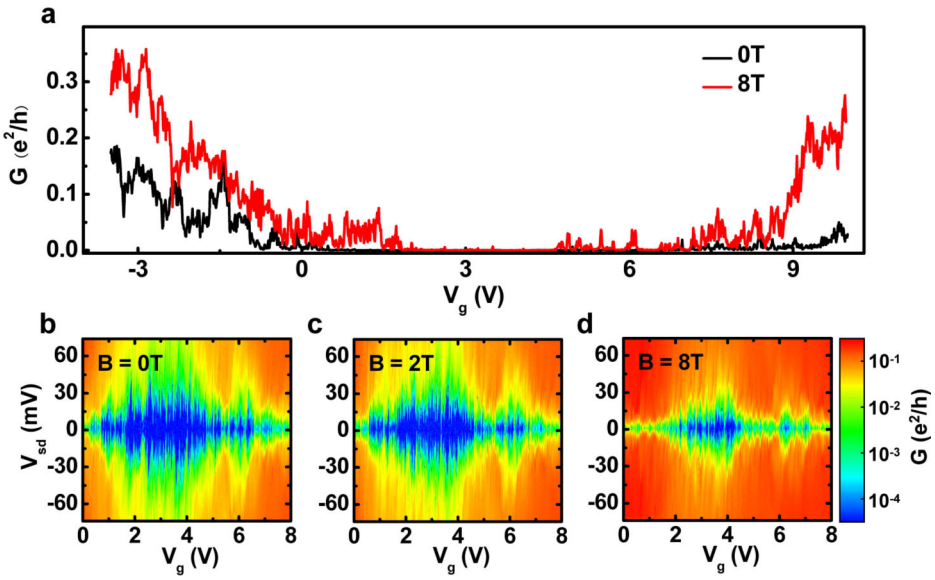

Figure 2. Electrical transport measurement of a graphene nanoribbon-FET with width of ~15 nm and length of 800nm

a, Differential conductance versus gate voltage with a magnetic field of 0 T (black) and 8 T (red) normal to the device plane. The measurements were carried out at 1.6 K. **b-d,** Differential conductance as a function of source-drain bias and back-gate voltage under magnetic field of 0 T (**b**), 2 T (**c**), and 8 T (**d**). These measurements show diamonds of suppressed conductance shrunk both in source-drain bias and gate voltage direction with increasing magnetic field.

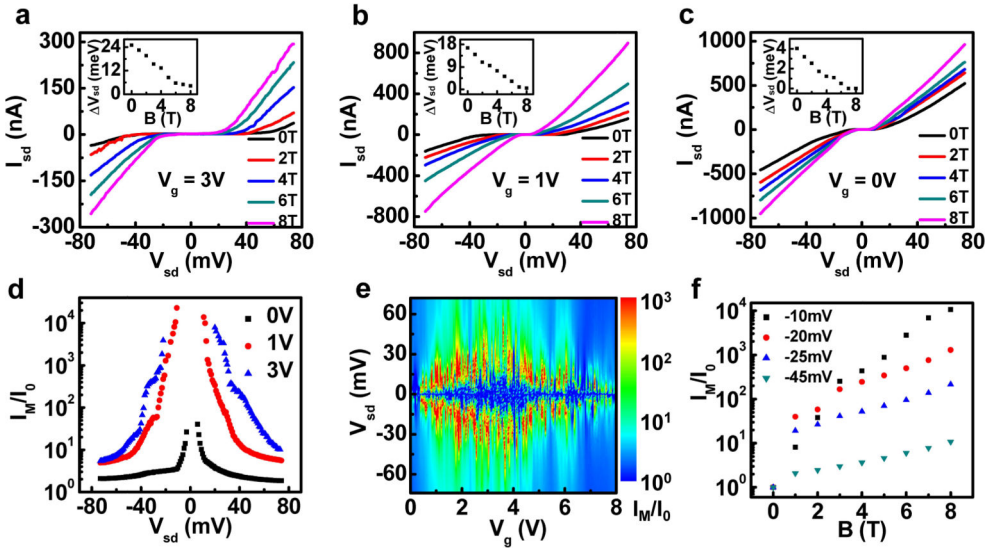

Figure 3. Tunable magnetoresistance in graphene nanoribbon-FET

a-c, The impact of magnetic field on current-voltage characteristics when the device is gated at V=3 V (**a**), 1 V (**b**) and 0 V (**c**). Each inset shows the source-drain gap (ΔV_{sd}) as a function of magnetic field. **d**, Current ratio *I*(8T)/*I*(0T) versus source-drain bias at V_g = 3 V. The middle interval for each plot is in the range of suppressed conductance which is beyond our equipment measurement limits. **e**, Current ratio *I*(8T)/*I*(0T) as a function of source-drain bias and gate voltage, highlighting huge increase of current under magnetic field when probing the device close to the diamond of suppressed conductance. **f**, Current ratio *I*(M)/*I*(0T) as a function of magnetic field when source-drain is biased at -10 mV, -20 mV, -25 mV and -45 mV at V_g = 1 V.

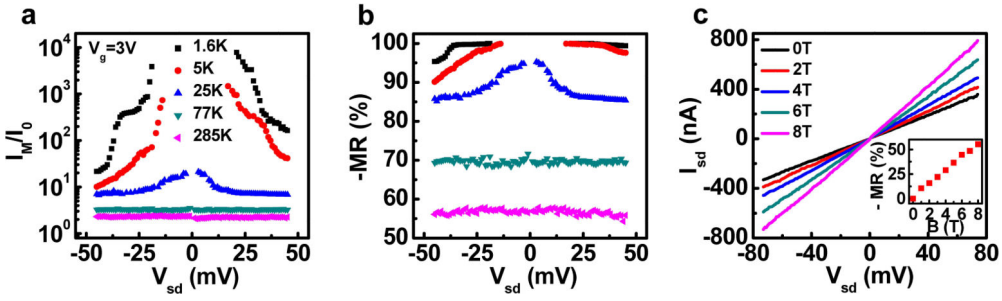

Figure 4. Temperature dependent magneto-transport properties

a-b, Current ratio *I*(8T)/*I*(0T) (**a**) and negative magnetoresistance (MR) (**b**) as a function of source-drain bias at 1.6 K, 5 K, 25 K, 77 K and 285 K. The device was gated at 3 V. **c,** Room temperature (285 K) *I-V* characteristic (V_g=3 V) at different magnetic field. The inset shows the negative magnetoresistance (MR) increases linearly with the applied magnetic field.

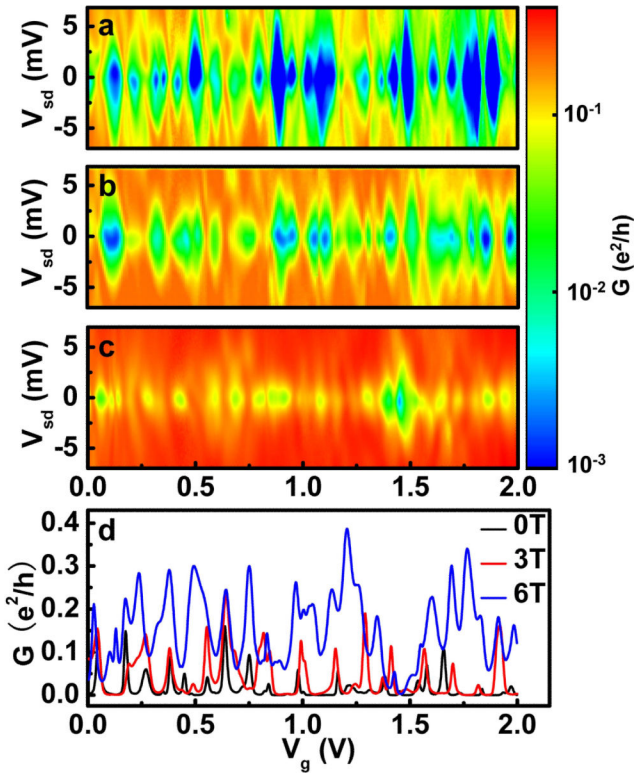

Figure 5. Magneto-transport properties of a short channel graphene nanoribbon-FET device with width 37 nm and length 200 nm

a-c, Differential conductance measurements as a function of source-drain bias and gate voltage at (**a**) 0 T, (**b**) T and (**c**) 6 T showing the evolution of diamond of suppressed conductance region with increasing magnetic field. **d,** Differential conductance (G) versus gate voltage at 0 source-drain bias at magnetic field of 0 T, 3 T and 6 T.